

# Probing Very High Energy Prompt Muon and Neutrino fluxes and the Cosmic Ray Knee via Underground Muons

Raj Gandhi <sup>1</sup> and Sukanta Panda <sup>2</sup>

*Harish-Chandra Research Institute,  
Chhatnag Road, Jhansi, Allahabad 211019, India.*

**Keyword:** Cosmic ray interactions, Muons, Charmed quarks

**PACS:** 13.85.Tp, 14.60.Ef, 14.65.Dw

## Abstract

We calculate event rates and demonstrate the observational feasibility of very high energy muons (1 TeV-1000 TeV) in a large mass underground detector operating as a pair-meter. This energy range corresponds to surface muon energies of  $\sim(5 \text{ TeV} - 5000 \text{ TeV})$  and primary cosmic ray energies of  $\sim(50 \text{ TeV} - 5 \times 10^4 \text{ TeV})$ . Such measurements would significantly assist in an improved understanding of the prompt contribution to  $\nu_e, \nu_\mu$  and  $\mu$  fluxes in present and future ultra-high energy neutrino detectors. In addition, they would shed light on the origin of and possible compositional changes at and around the observed 'knee' in the cosmic ray spectrum.

## 1 The Cosmic Ray Spectrum and the Knee

Cosmic ray studies, with the spectrum extending over ten decades in energy, have proved to be fertile terrain for furthering our knowledge of both astrophysics and particle physics ( reviews may be found in [1, 2, 3, 4]). They have traditionally provided us with clues for the existence of new particles and the physics associated with them, which have later been confirmed by detailed accelerator experiments. In fact, prior to 1950 and the advent of modern accelerator technology, they provided the only means of studying high-energy particle production and interactions. Additionally, as a result of our attempts to understand the origin of cosmic rays, they have contributed to our knowledge of acceleration via shocks, and the propagation of charged particles in the galaxy and heliosphere.

The cosmic ray spectrum, characterised by a steeply falling power-law behaviour over its entire range, exhibits two transition regions where the slope changes noticeably:

- A steepening of the spectrum occurs around  $E \approx 5 \times 10^6 \text{ GeV}$ , *i.e.* the index  $\gamma$  describing the power-law behaviour of the differential flux,  $dN/dE \sim E^\gamma$ , changes from  $\gamma \approx -2.7$  to  $\gamma \approx -3.1$ ; leading to the feature called the 'knee'.

---

<sup>1</sup>Email: raj@mri.ernet.in

<sup>2</sup>Email: sukanta@delta.ft.uam.es, Present address: Dpt. de Fisica Terica and Instituto de Fisica Terica, Universidad Autonoma de Madrid, Madrid, Spain

- A flattening of the spectrum occurs around  $E \approx 5 \times 10^9$  GeV, *i.e.* at the “ankle”; with the index  $\gamma$  changing back to  $\sim 2.4 - 2.7$ . Beyond the ankle, in the realm of ultra high energy cosmic rays, data [5, 6, 7] is sparse and conflicting, but highly intriguing. While we will not address the interesting puzzle in this regime here, a discussion of the various issues may be found in [8, 9], and a recent assesment of the shape of the spectrum based on current knowledge can be found in [10].

The physical reason for the existence of the knee is at present an unresolved problem of great significance to understanding the origin of galactic cosmic rays. It is generally believed that the reasons underlying this distinctive shift in the spectrum are astrophysical in nature, as opposed to those stemming from a change in hadronic interactions at these energies which, at present, are not within the reach of existing accelerators. This conclusion is based on the observed correspondence between independant measurements of the muon number spectrum, Cerenkov radiation and hadronic constituents of air-showers [11, 12, 13, 14, 15]. While the reasons for the shift in the spectrum remain un-understood, these data exhibit an expected co-relation which supports the absence of radically different physics interactions at these energies.

While the case for the existence of new physics being at least partially responsible for a shift in the spectral index is not wholly without motivation<sup>3</sup>, we stress that it appears unlikely that this can be empirically corroborated or refuted in the near future in CR measurements. This is because, as we shall discuss below, uncertainties (in the knee region) in the CR composition and prompt muon and neutrino contributions would likely overshadow evidence of such new interactions. In any case, this hypothesis will be thoroughly probed in the near future by the Large Hadron Collider (LHC) at CERN which will operate at a center of mass energy of  $\sqrt{s} = 14$  TeV.

## 2 Uncertainties in the Muon and Neutrino Fluxes in the Knee region and beyond

As stated earlier, present data [20] when culled and correlated, appear to favour one or more astrophysical reasons for the existence of the knee. These include it being a rigidity-dependant effect (originally proposed in [21]) related to the (different) maximum acceleration energies for different nuclei either in the cosmic ray source itself or during the propagation process. Data from surface air-showers and optical detectors indicate, without being conclusive, that the average mass of the cosmic ray spectrum nuclei differs before and after the steepening at the knee. In particular, there appears to be some evidence[22, 23] that the composition is heavier above the knee region. If this is true, then, as discussed in [24], significant suppression of the very high energy ( $\geq 10^5$  GeV) muon and neutrino fluxes resulting from CR interactions in the atmosphere and in the interstellar medium can occur.

A second major factor in determining the enhancement (or lack thereof) of muon and neutrino fluxes above several TeV are the uncertain magnitudes of the prompt (*i.e.* those resulting from heavy meson decay, notably, charm mesons and heavier composites) fluxes of both. At low (*i.e.*

---

<sup>3</sup>This region in  $E_p$ , (*i.e.* the energy of the primary particle) corresponds to several TeV in center of mass energies. Thus there are many conjectures for physics beyond the Standard Model which come into play, *e.g.* SUSY, technicolour, large extra dimensions etc. These could lead (via new particle production and decay) to energy being channelled into muons, neutrinos or other secondary particles in a manner that present cosmic ray experiments are insensitive to, causing the shift in the (measured) energy spectrum [16, 17, 18, 19].

$\sim$  GeV) energies, the cosmic ray induced neutrino and muon fluxes receive their dominant contributions from the decays of  $\pi$  and  $K$  mesons, whose interaction lengths significantly exceed their decay lengths [45, 46, 47, 48]. (These fluxes are henceforth referred to as the conventional fluxes in what follows.) This situation changes at  $\sim$  TeV energies, and secondary interactions of these particles become possible, leading to the production of heavy short lived hadrons. While upper bounds on the flux of muons and neutrinos have been provided by several experiments *e.g* LVD [49], AKENO [50] and AMANDA [51], they still allow for a very large possible range of prompt flux magnitudes.

Present phenomenological predictions for the diffuse fluxes of these prompt muons and neutrinos can differ by about two orders of magnitude [48, 52, 53, 54, 55, 56, 57]. The sources of this large uncertainty lie, to a significant extent, in the choice of charm production models. For instance, differing predictions arise from models based on perturbative QCD (pQCD) with a  $K$  factor [48], next-to-leading order (NLO) pQCD [56, 54], quark-gluon string models and recombination quark-parton models [55] etc. In general, QCD based models must contend with a large uncertainty associated with the extrapolation of the gluon parton distribution function  $g(x)$  to small fractional momentum  $x < 10^{-5}$ . Theoretical models generally assume

$$xg(x) \sim x^{-\lambda},$$

where  $\lambda$  is in the range  $0 - 0.5$ , and fluxes depend strongly on the chosen value of  $\lambda$ . We note that depending on the model, the prompt muon and neutrino fluxes from charm decay exceed the corresponding conventional fluxes (from  $\pi$  and  $K$  decays) somewhere between (surface) muon energies of few tens of TeV and few PeV [56]. Reliable measurements of muon fluxes in this range would thus, at the very least, help in establishing the reliability of a particular class of models.

While we do not give a detailed account of the flux predictions from all the different models, we attempt to give a representative idea in our calculations of the variation possible even within a given charm production model. While the conventional muon flux from  $\pi$  and  $K$  decays is well understood and fairly firm, the prompt flux predictions are subject to variations resulting from different parton distribution functions and choices of the factorization and renormalisation scales as mentioned above. We thus stress the need for better empirical determination of the muon (and associated neutrino fluxes) in this region, a topic which is elaborated upon in the next section.

### 3 The significance of measurements of the muon and neutrino fluxes in the knee region

With very few exceptions, available data on muons above several TeV comprise of measurements of the number spectrum rather than the energy. This is primarily due to the size and density requirements imposed on detectors by the significant penetration lengths achieved by high energy muons.

The desirability of improved and statistically significant muon energy measurements in the few TeV to few hundred TeV region stems from (at least) three reasons:

- As mentioned above, the physical origin and composition of cosmic rays in this energy range is currently obscured by a paucity of data on VHE muon and neutrino fluxes. Observations would thus certainly illuminate the current debate on the reason for the occurrence of and compositional changes at the knee.

- Also, as discussed above, QCD related theoretical uncertainties dominate the predictions of the prompt contribution to muon and neutrino fluxes. As emphasized in [56, 58], the measurement of down-going muon fluxes would provide a valuable handle in their reduction.
- Both the conventional and prompt muon fluxes at these energies are closely related to the associated neutrino fluxes. For prompt contributions, this is because the kinematics of charmed particle decay and the corresponding semi-leptonic branching ratios ensure that the  $\nu_e$  and  $\nu_\mu$  fluxes are identical upto a few percent to the muon fluxes in this energy range, regardless of the choice of the charm production model or of  $\lambda$ . The conventional neutrino flux, on the other hand, is about 10 % of the conventional muon flux. At the energies of interest here, neutrinos resulting from cosmic ray interactions in the atmosphere and in the inter-stellar medium constitute the most important background to searches for diffuse fluxes of ultra high energy (UHE) neutrinos [32, 33, 34, 35, 36, 37, 38] from cosmological sources (*e.g.* active galactic nuclei, gamma-ray bursts etc.) in neutrino telescopes like AMANDA [39], ICECUBE [40] and NEMO [41]. Thus, they are an important obstacle to the much-anticipated detection of such energetic point sources in these detectors. Empirical data on downgoing muons from cosmic rays would prove invaluable in understanding this background to the UHE neutrino signal, since it can be co-related to the neutrino flux.

In the context of the points above, it is relevant to stress the importance of being able to disentangle the prompt (due to the decay of produced heavy mesons) and conventional (from  $\pi$  and  $K$  decays) and diffuse UHE (from extra-galactic sources) contributions to the neutrino fluxes. Methods to enable this have been studied, and are based on the differences in zenith angle, depth and spectral dependence between these fluxes [42, 43] and on the isolating capability of showering  $\nu_e$  charged current events via a break in the spectrum [44].

Having emphasized the importance of muon energy measurements in the several TeV to several hundred TeV range, we proceed in the next section to study the potential of the *pair meter* method [25, 26, 27] as applied to such measurements made in a *large iron calorimeter* (50 kT) <sup>4</sup>. Since individual muon energies will become measurable using this technique, it will be possible to augment the sparse existing data on cosmic ray muons in the important range where they have *surface* energies of  $\approx 5 - 5000$  TeV. Furthermore, these observations can be combined with balloon-based experiments (*e.g.* TRACER [29]) and upcoming hybrid air-shower experiments (*e.g.* KASCADE-Grande [30] and LOPES [31]) to enhance our understanding of the issues discussed above. We mention here that this range in *muon surface energy* roughly corresponds to a range of  $50 - 5 \times 10^4$  TeV in *primary cosmic ray energy*, which is crucial to an enhanced understanding of the origin of the knee.

In the remainder of the paper, we first provide a discussion of the pair-meter technique and the pair production cross section which results in the observed cascades. This is followed by a brief description of a typical large-mass iron calorimeter. Subsequent to this we summarize the interactions and losses of muons in matter enroute to an underground detector, and their incorporation into our calculation. We then calculate anticipated event rates for a 50 kT detector and demonstrate that even after accounting for energy losses in the surrounding rock, event rates can be appreciably large for the 1 – 1000 TeV range, corresponding to *surface* muon energies in the range of several TeV to several PeV.

---

<sup>4</sup>Such a detector is currently being planned for location in India [28]

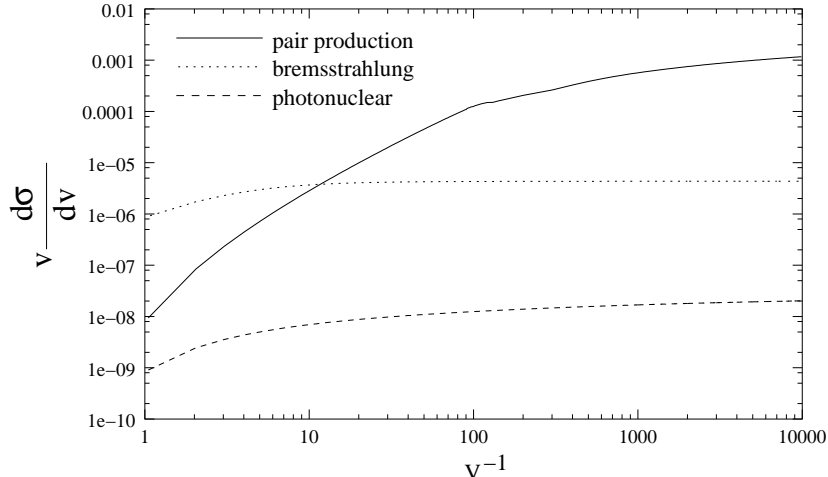


Figure 1: Differential cross section  $v d\sigma/dv$  vs.  $v^{-1}$  (inverse of the relative energy transfer) for pair production (solid)[59], bremsstrahlung (dotted)[61] and photonuclear (dashed)[62] processes.

## 4 The Pair Meter method and the associated Pair Production Cross Section

Due to the penetrating power of muons, their energy measurements require techniques which differ from those employed for photons, hadrons and electrons. Furthermore, muon energy measurement methods which work well in the GeV range (magnetic spectrometry or measuring Cerenkov radiation) are rendered impractical in the TeV range primarily due to requirements of size imposed by the combination of high energies and a steeply falling spectrum.

The pair meter technique[25, 26, 27] skirts some of the disadvantages of traditional muon detectors by relying on a somewhat indirect method, *i.e.* the measurements of the energy and frequency of electron-positron pair cascades produced by the passage of a high energy muon in dense matter. A reliable reconstruction of the muon energy in this method is based on the following:

- The cross section for  $e^+e^-$  pair production by a muon with energy  $E_\mu$  with energy transfer above a threshold  $E_0$  grows as  $\ln^2(2m_e E_\mu/m_\mu E_0)$ , where  $m_\mu$  and  $m_e$  are the muon and electron masses respectively.
- Defining  $v = E_0/E_\mu$ , above  $v^{-1} = 10$ , this cross section dominates those for other muon energy loss processes which generate observable cascades in its passage through dense matter, *e.g.*  $\mu - N$  inelastic scattering and bremsstrahlung emission. This is demonstrated in Figure 1, where we compare the differential cross sections for these various interactions as a function of  $v^{-1}$ .
- The energy lost to each cascade resulting from  $e^+e^-$  pair production is a very small fraction (about  $10^{-2}$ ) of the muon energy for the range of  $v^{-1}$  which we focus on here.
- The dependance of the pair production cross section on  $E_\mu/E_0$  then allows one to infer the muon energy by counting the number of interaction cascades  $N$  in the detector with energies above a threshold  $E_0$ .

We now make the above statements more precise. In the approximations

$$v = \frac{E_0}{E_\mu} \ll \frac{2m_e}{m_\mu}$$

and

$$E_0 \gg 2m_e 189\sqrt{e}Z^{-1/3} \simeq 0.3Z^{-1/3}\text{GeV},$$

( $Z$ =atomic number= 26, for iron) both of which are valid for the choice of  $E_0, E_\mu$  for which we present results below, the expression for the differential pair production cross section is given by[59]

$$v \frac{d\sigma}{dv} \simeq \frac{14\alpha}{9\pi t_0} \ln \left( \frac{\kappa m_e E_\mu}{\epsilon m_\mu} \right), \quad (1)$$

where  $\alpha = 1/137$  and  $\kappa \simeq 1.8$ .  $t_0$  is the radiation length (r.l) which is given by

$$t_0 = \left( \frac{4Z(Z+1)}{A_W} \alpha r_0^2 N_A \ln(189Z^{-1/3}) \right)^{-1}. \quad (2)$$

Here  $A_W$  is the gram atomic weight (for iron, this is 56 grams),  $r_0$  is the classical electron radius and  $N_A$  the Avogadro number. For iron, this gives  $t_0 = 13.75 \text{ gm/cm}^2$ .

The average number of interaction cascades  $M$  above a threshold  $E_0$  for  $v \leq 10^{-3}$  is given by

$$M(E_0, E_\mu) = T t_0 \sigma(E_0, E_\mu), \quad (3)$$

where  $T$  is the thickness of the target in units of  $t_0$  and  $\sigma(E_0, E_\mu)$  is the integrated cross section (in units of  $\text{cm}^2/\text{gm}$ ),

$$\sigma(E_0, E_\mu) \simeq \frac{7\alpha}{9\pi t_0} \left( \ln^2 \left( \frac{\kappa m_e E_\mu}{E_0 m_\mu} \right) + C \right), \quad (4)$$

where  $C \simeq 1.4$ .

At this point it is important to mention that the capability and effectiveness of the pair meter method for high energy muons has been tested and demonstrated by the NuTEV/CCFR collaboration, as described in [60]. The calculations which follow are performed for a 50 kT iron calorimeter. Our prototype is based on the suggested design for INO; see [28] for details. The dimensions of a 50 kT detector of this type would correspond to (approx)  $15 \text{ m} \times 15 \text{ m} \times 45 \text{ m}$ . A muon traversing a 20 m path in this detector corresponds to a path-length of  $\sim 1145$  r.l. In what follows, we assume a (conservative) ‘‘average’’ path-length of 1000 r.l for the typical muon and calculate the number of observable cascades produced by it, for different cascade thresholds and muon energies. Figure 2 shows the average number of cascades above a threshold energy  $E_0$  produced by a muon entering the detector with energy  $E_\mu$  and  $T = 1000$  r.l.; for three different choices of  $E_0$ , *i.e.* 1 GeV, 10 GeV and 100 GeV. Quantitatively, we note that this leads to a  $E_\mu = 100$  TeV muon generating approximately 40 cascades, each of energy greater than  $E_0 = 10$  GeV and 10 cascades with energy in excess of 100 GeV. By counting the cascades for several choices of thresholds for a traversing muon, one obtains a reliable estimate of its energy.

It is also relevant to remark here that the relative energy measurement error,  $\delta E_\mu/E_\mu$  in the pair meter is given by

$$\delta E_\mu/E_\mu = \sqrt{\frac{9\pi}{28\alpha T}} \simeq \sqrt{\frac{137}{T}}. \quad (5)$$

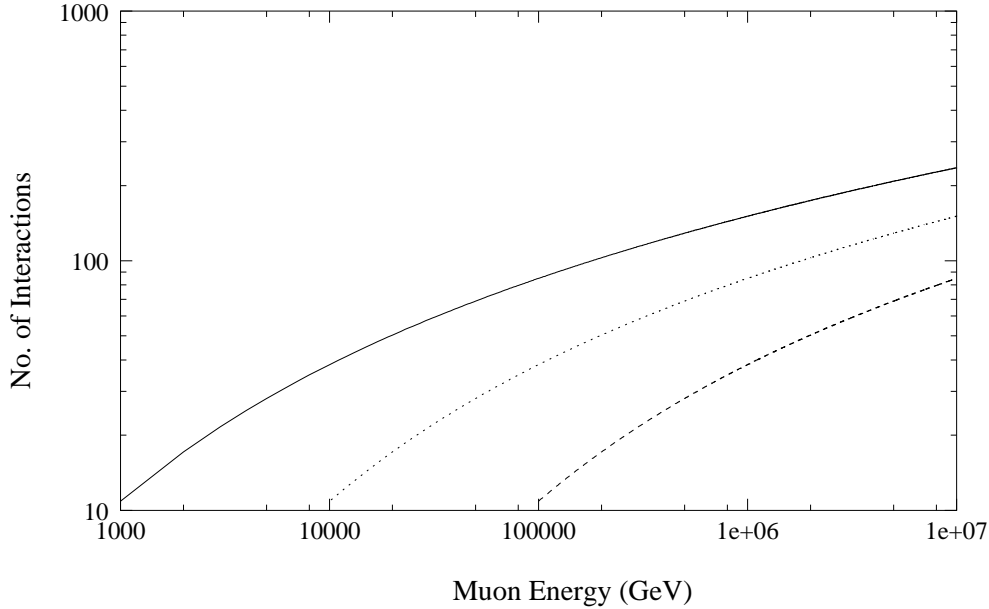


Figure 2: Average number of cascades above a threshold  $E_0$  vs. muon energy for  $E_0 = 1$  GeV (solid line), 10 GeV (dotted) and 100 GeV (dashed), with  $T$  fixed to 1000 r.l.

For  $v = (10^{-3} - 10^{-2})$ , which is the range we focus on here, this allows a liberal tolerance for error in the measurements of individual cascade energies. We note also that the errors do not worsen with increasing muon energy, which is an important advantage of the pair-meter technique.

## 5 The Surface Muon Energy determination for Underground Events

It is important to co-relate the measured muon energies in an underground detector to their surface energies, which we take to be those that would be observed were our detector placed on the surface of the earth. This requires a calculation of the energy loss as the muon traverses the rock between the earth's surface and the detector.

These losses originate from ionization, bremsstrahlung, pair production and photonuclear interactions. They can be effectively parametrized [59, 61, 62] for  $E_\mu \geq 1$  TeV, since the average loss increases predominantly linearly with energy,

$$\left\langle \frac{dE}{dX} \right\rangle = -\alpha - \beta E, \quad (6)$$

where  $\alpha$  parametrizes the contribution from ionization of muons and  $\beta$  encapsulates the contribution from bremsstrahlung, pair production and photonuclear processes. Note that  $\alpha$  and  $\beta$  carry a very weak (intrinsic) energy dependence. It is thus appropriate to assume that the average muon energy at depth  $X$  is

$$\langle E_\mu(X) \rangle = \left( E_\mu^s + \frac{\alpha}{\beta} \right) e^{-\beta X} - \frac{\alpha}{\beta}, \quad (7)$$

where  $E_\mu^s$  is the initial surface muon energy. One may use this to write down the minimum surface

energy required of a muon to reach a depth  $X$  as,

$$E_{min}^s = \frac{\alpha}{\beta} (e^{\beta X} - 1) . \quad (8)$$

From Eq. 7, we get the relation between initial energy  $E_\mu^s$  and degraded energy of muon  $E_\mu$  after travelling a distance  $X$  as,

$$E_\mu^s = \left( E_\mu + \frac{\alpha}{\beta} \right) e^{\beta X} - \frac{\alpha}{\beta} . \quad (9)$$

The differential muon flux at a depth  $X$  is given by,

$$\frac{dN}{dE_\mu} = \frac{dN}{dE_\mu^s} e^{\beta X} . \quad (10)$$

where  $\frac{dN}{dE_\mu^s}$  is the initial muon flux with surface muon energy  $E_\mu^s$ .

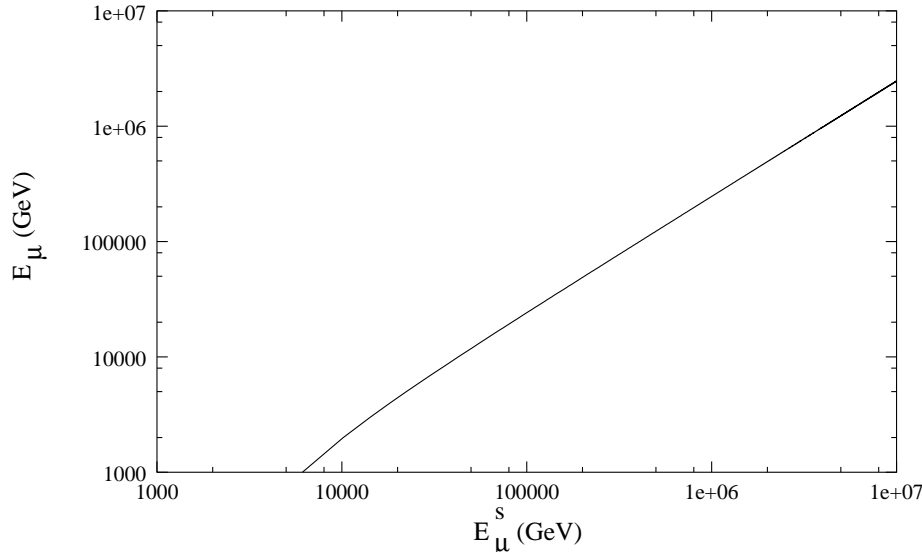


Figure 3: Degraded muon energy,  $E_\mu$  vs. surface muon energy,  $E_\mu^s$  after passing a depth of  $3.5 \times 10^5 g/cm^2$ , corresponding to the proposed INO location.

The  $\alpha$  and  $\beta$  in the analytical expression can be obtained for standard rock. The depth relevant to the INO detector's proposed location is  $3.5 \times 10^5 gm/cm^2$ . The values are,

$$\beta = 4 \times 10^{-6} cm^2/g, \quad \frac{\alpha}{\beta} = 675 GeV. \quad (11)$$

Figure 3 shows the degraded muon energies (*i.e.* those measured for muons entering the detector after traversing the rock) vs their corresponding surface energies after losses are accounted for in the manner described above. We note that typically,  $E_\mu^s \simeq (2 - 5) \times E_\mu$ .

Flux model	PDF	Scales	a	b	c	d
PRS1	CTEQ3	$\tilde{M} = \tilde{\mu} = m_c$	5.37	0.0191	0.156	0.0153
PRS2	CTEQ3	$\tilde{M} = 2\tilde{\mu} = 2m_c$	5.79	0.345	0.105	0.0127
PRS3	D	$\tilde{M} = 2\tilde{\mu} = 2m_c$	5.91	0.290	0.143	0.0147

Table 1: PRS parameters for the prompt muon and antimuon fluxes.  $m_c$  is the mass of the charm quark.

$E_\mu(TeV)$	Number of muons per solid angle entering the detector in 5 years					
	conv+TIG	conv	TIG	PRS1	PRS2	PRS3
1	$1.035 \times 10^7$	$1.03 \times 10^7$	37461	55482	95489	136871
10	52486	51282	1204	2952	5341	10443
50	770	696	74	236	431	1104
100	127	106	21	73	134	387
200	22	16	6	22	40	129
300	8	5	3	11	19	66
400	4	2	2	6	11	41
500	2	1	1	4	7	28
600	1.5	1	.5	3	5	20
700	1	.5	.5	4	7.5	31
800	.8	.35	.5	1.5	3	12
900	.65	.25	.37	1.25	2.5	10
1000	.5	.2	.3	1	2	4
10000	.0025	.0003	.0022	.007	.013	.08

Table 2: Number of muons per solid angle entering the detector over 5 years for various energies of the entering muon,  $E_\mu$ .

## 6 Muon Fluxes

Extensive predictions and studies [45, 46, 47, 48, 52, 53, 54, 55, 56, 57] for prompt cosmic ray muon fluxes at very high energies exist in the literature, as mentioned earlier. For our representative calculations of muon event rates, we have used the relatively conservative predictions for charm induced fluxes given in [48, 54]. The large variation in muon rates possible due to flux uncertainties even when these fluxes are used is amply reflected in our results, most noticeably in Table 2. One would expect much larger variations if the full range of prompt flux models available is used to calculate event rates.

In [48] (henceforth referred to as the TIG flux), the conventional and prompt fluxes have been parametrized as

$$\frac{dN}{dE} = \frac{N_0 E^{-\gamma-1}}{1 + AE} \quad (12)$$

for  $E < E_a$ . and as

$$\frac{dN}{dE} = \frac{N'_0 E^{-\gamma'-1}}{1 + AE} \quad (13)$$

for  $E > E_a$ . For the conventional muon flux  $N_0 = 0.2$ ,  $N'_0 = 0.2$ ,  $\gamma = 1.74$ ,  $\gamma' = 2.1$ ,  $E_a = 5.3 \times 10^5$ ,  $A = 0.007$ .

		Number of cascades per muon for different thresholds $E_0$ in GeV								
$E_\mu$	$E_\mu^s$	5	10	20	50	100	300	500	1000	5000
1	6.1	3.08	2.56	3.78						
10	40.26	17.28	10.99	6.43	3.08	2.56				
20	83.16	25.3	17.28	10.99	5.34	3.08				
50	205	38.58	28.26	19.67	10.99	6.43	2.78	2.56		
100	407.58	50.63	38.58	28.26	17.28	10.99	4.58	3.08	2.56	
200	813	64.43	50.63	38.58	25.30	17.28	8.11	5.34	3.08	
300	1218	73.3	58.49	45.42	30.8	21.76	10.99	7.46	4.19	
400	1624	79.96	64.43	50.63	35.06	25.3	13.39	9.33	5.34	
500	2029	85.33	69.24	54.89	38.58	28.26	15.45	10.99	6.43	2.56
600	2435	89.85	73.3	58.49	41.58	30.8	17.28	12.47	7.46	2.58
700	2841	93.76	76.83	61.64	44.21	33.05	18.91	13.82	8.43	2.6
800	3246	97.23	79.96	64.43	46.56	35.06	20.4	15.06	9.33	2.72
900	3652	100.33	82.77	66.95	48.69	36.9	21.76	16.21	10.18	2.89
1000	4057	103.16	85.33	69.24	50.63	38.58	23.02	17.28	10.99	3.08
10000	40554	174.84	151.24	129.38	103.16	85.33	60.63	50.63	38.58	17.28

Table 3: Number of cascades above thresholds  $E_0 = 5, 10, 20, 50, 100, 300, 500, 1000, 5000$  GeV per muon. Here  $E_\mu$  is the energy of the muon in TeV entering the detector, and  $E_\mu^s$  is its corresponding energy in TeV at the surface of the earth, assuming it traversed a depth of rock corresponding to  $3.5 \times 10^5 gm/cm^2$ .

For the prompt muon flux  $N_0 = 1.4 \times 10^{-5}$ ,  $N'_0 = 4.3 \times 10^{-4}$ ,  $\gamma = 1.77$ ,  $\gamma' = 2.01$ ,  $E_a = 9.2 \times 10^5$ ,  $A = 2.8 \times 10^{-8}$ .

The second set of representative prompt muon fluxes we use are calculated in [54] (henceforth referred to as the PRS1, PRS2 and PRS3 fluxes). The differences in the three fluxes originate in different choices of parton distribution functions (PDF) and factorisation ( $\tilde{M}$ ) and renormalisation scales ( $\tilde{\mu}$ ) of the theory. These fluxes can be conveniently parametrized [54] as follows

$$\frac{dN}{dE} = 10^{-a+bx+cx^2-dx^3}, \quad (14)$$

where  $x = \text{Log}_{10}(E/\text{GeV})$ , with  $a, b, c$  and  $d$  as in Table.1.

In Figure 4 we show the conventional (TIG) and prompt (TIG and PRS) surface muon fluxes. Uncertainties in the conventional flux, unlike the prompt case, are not major, hence we have shown only the TIG parametrization. We note that depending on the flux model, the prompt fluxes rise above the conventional flux for (surface) muon energies between 200 TeV and 1000 TeV. In terms of (degraded) muons entering the detector, we see from Figure 3 and Figure 5 that this corresponds to measured muon energies of several tens of TeV and several hundreds of TeV. Thus, we note that underground muon measurements in this range will help reduce the present uncertainties in deducing the charm contributions to muon and neutrino fluxes. Our calculations provide a quantitative estimate of the feasibility and the potential of these measurements to accomplish this.

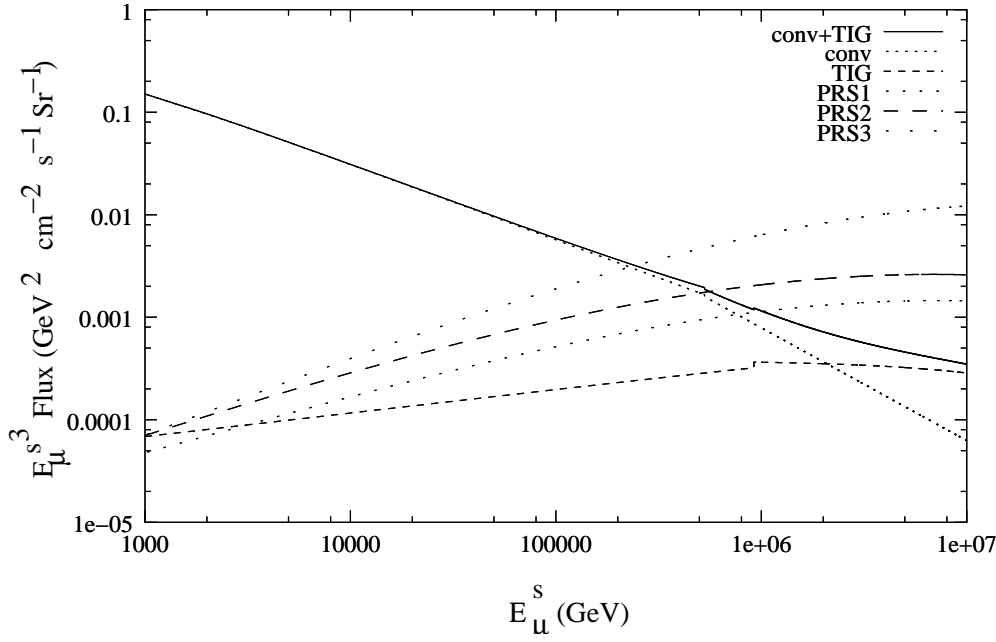


Figure 4:  $(E_\mu^{s3} \times \text{Flux})$  vs. surface muon energy  $E_\mu^s$  for total TIG flux(solid), conventional(dotted), TIG prompt (short dashed), and prompt fluxes corresponding to PRS1(short spaced dots), PRS2(large dashed) and PRS3(large spaced dots).

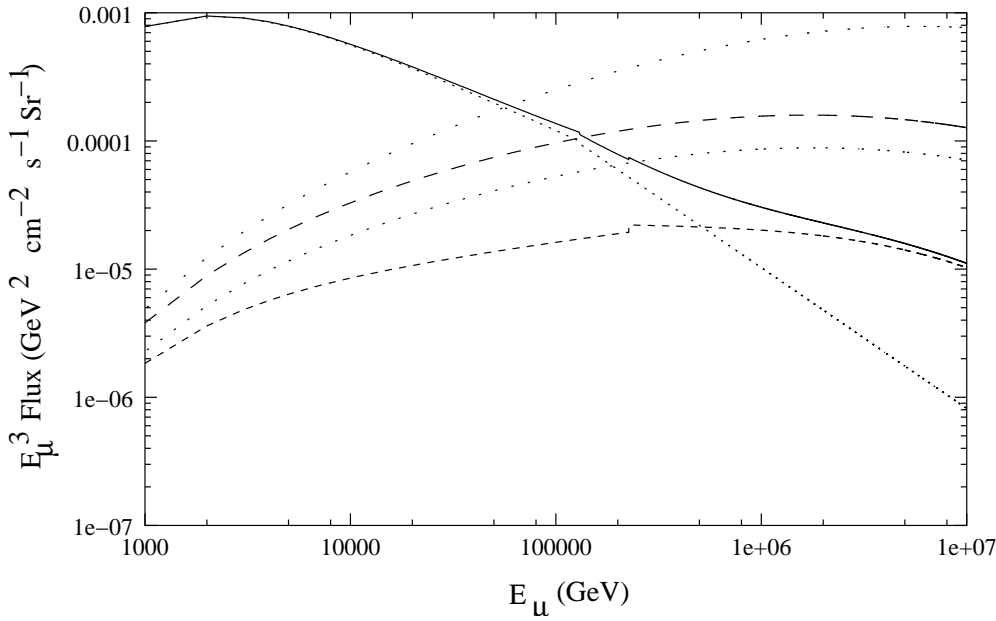


Figure 5:  $(E_\mu^3 \times \text{Flux})$  vs. energy of muon entering the underground detector  $E_\mu$ , ( for the flux models listed in the previous figure) after passing through the rock distance of  $3.5 \times 10^5 \text{ gm/cm}^2$ . . Labelling of plots is identical to figure 4.

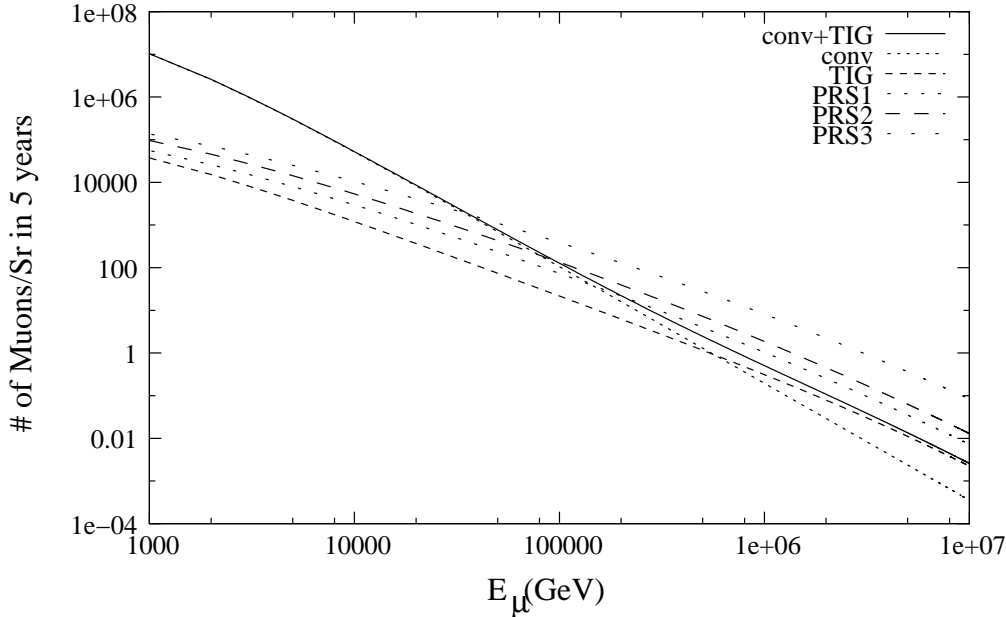


Figure 6: Number of muons entering the 50 kT detector in 5 years per solid angle vs. muon energy. Energy losses in the surrounding rock are taken into account. Depth of the detector is assumed to be  $3.5 \times 10^5 g/cm^2$ .

## 7 Results and Discussion

We are now in a position to calculate the expected cascade events for a 50 kT detector in the energy range of interest discussed above. While an entering muon in this energy range will produce observable cascades, the number entering the detector over a given period is limited by the sharply falling fluxes at these energies. It is thus pertinent to obtain a quantitative measure of this by estimating  $n_\mu$ , the number of muons above a given threshold entering the detector per steradian for an exposure of  $t$  years,

$$n_\mu = \int_{E_{th}}^{\infty} dE_\mu \frac{dN}{dE_\mu} A \times t, \quad (15)$$

where  $A$  is the exposed area of a 50 kT iron detector. This is shown in Figure 6 and Table 2. We note that while the number of entering muons for the lowest energy in Table 2, *i.e.* 1 TeV is very large, one also obtains an observable number, *i.e.* 1-3 events after integrating over solid angle (considering that there is no “back-ground” as such for such events) over the 5 year period even for  $E_\mu = 1000$  TeV for the most conservative flux choice (TIG). These energies delineate the muon energy range accessible. The number of entering muons for all choices of PRS fluxes will be substantially higher, as shown. Even for the most conservative (TIG) flux choice, one expects good observational capability upto several hundred TeV<sup>5</sup>.

The number of cascades per muon above  $E_0=5, 10, 20, 50, 100, 300, 500, 1000, 5000$  GeV respectively using Eq. 3 and 4 are tabulated in Table 3. Table 3 also lists the surface muon energy  $E_\mu^s$  corresponding to the underground muon energies  $E_\mu$ . While these are sample choices, it is clear

<sup>5</sup>We have given the per-steradian rates here. In order to predict the rate integrated over angle, predictions must carefully take into account the depth dependance of the fluxes for a particular detector and its surrounding topography.

that they can be further optimized based on the muon energy that one wants to observe to good statistical accuracy.

The *total* number of cascade events per ster-radian  $N_c(E_0)$  (above a given threshold  $E_0$  and for a  $50 \text{ kT} \times 5 \text{ yr}$  exposure) is given by

$$N_c(E_0) = M(E_\mu, E_0)n_\mu, \quad (16)$$

where  $M(E_\mu, E_0)$  is the cascade number calculated above in Section 2.1. From Table 2 and Table 3, we observe that this number is considerable for most thresholds, promising rich observational capabilities. For example, for the (most conservative) conventional+TIG flux model which we use as our benchmark, one finds that at even at muon energies of 1000 TeV, one can produce 51 events per solid angle for a threshold of 5 GeV and  $\sim 1$  event per solid angle for a threshold of 5000 GeV. Expectedly, the PRS models predict significantly more events compared to these estimates.

We have used the TIG flux as a benchmark to establish observability, since it leads to the most conservative event rate predictions. All other flux parametrisations lead to higher predictions. We note that even though TIG and PRS are not vastly different from each other in a qualitative sense since both are based on perturbative QCD inputs, their event rates in a large mass pair meter differ significantly. Indeed, the variations amongst fluxes in the same family (PRS1, PRS2, PRS3) are also large. Thus, the muon event rate can act as a soft (*i.e.* not definitive, given the large uncertainties in the QCD predictions) discriminator between various prompt flux models and provide pointers to the physics input that should guide their development. Similarly, this rate provides a tool to better understand the present spectral uncertainties in the cosmic ray knee origin.

## 8 Conclusions

Our main results are presented in Figs 6 and 2 and Tables 2, 3. From these we (conservatively) conclude that underground muon energy measurements for an energy range of  $E_\mu$  of 1-1000 TeV are possible with a 50 kT iron detector <sup>6</sup> running for 5 years. This will enable a better handle on the very high energy muon fluxes between several TeV to about 5 PeV, and consequently illuminate our estimates of the background muon and neutrino fluxes for ultra high energy neutrino detectors and lessen present uncertainties in charm production models. As emphasized earlier, the prompt muon flux is a measure of the prompt  $\nu_e$  and  $\nu_\mu$  flux, hence its importance to ultra high energy neutrino astronomy cannot be underestimated.

The observable muon energy range discussed in our results also corresponds to a range of 50 TeV to 50 PeV in *primary cosmic ray energies*. This range is crucial to an understanding of the origin of knee and our calculations demonstrate the feasibility and potential resulting from muon measurements for a better understanding of the origin of the knee.

A detailed and comprehensive set of predictions for a given large mass detector necessarily requires a much more elaborate calculation of the muon losses than what is presented here, since local topography plays an important role in determining the surface muon energy corresponding to a measured muon energy. Our aim in this paper has been more to demonstrate observational feasibility rather than to make precise predictions. Thus the calculations here show that very high energy muon measurements are possible in a large iron calorimeter and can aid in illuminating

---

<sup>6</sup>As stated earlier, we have used a depth corresponding to the proposed INO site for specificity, however, the results can be easily generalised to other depths, as should be obvious.

three important outstanding questions which address partially overlapping issues, one in cosmic ray physics, the second in theoretical QCD and the third in ultra high energy neutrino astronomy.

**Acknowledgment:** We thank Namit Mahajan for helpful discussions. RG would also like to thank Francis Halzen for informative discussions and John Beacom for pointing out some helpful references.

## References

- [1] V. S Berezinsky, S. V Bulanov, V. A. Dogiel, V.L. Ginzburg and V.S. Ptuskin, *Astrophysics of Cosmic Rays*, (North Holland, Amsterdam) 1990.
- [2] T.K. Gaisser, *Cosmic Rays and Particle Physics*, (Cambridge University Press, Cambridge) 1990.
- [3] M.S. Longair, *High Energy Astrophysics*, (Cambridge University Press, Cambridge) 1992.
- [4] T. Stanev, *High Energy Cosmic Rays*, (Springer-Praxis, Berlin) 2003.
- [5] M. Nagano and A.A. Watson, *Rev. Mod. Phys.* **72**, 689 (2000).
- [6] HiRes-MIA Collaboration, T. Abu-Zayed *et al*, *Phys.Rev.Lett.* **92**, 151101 (2004), [astro-ph/0208243].
- [7] AGASA Collaboration, M. Takeda *et al* *Astropart.Phys.* **19**, 447 (2003).
- [8] P. Bhattacharjee and G. Sigl, *Phys. Reports* **327**, 109 (2000); *Astropart. Phys.* **16**, 373, (2000).
- [9] F. Halzen and D. Hooper, *Rept. Prog. Phys.* **65**, 1025 (2002).
- [10] D. De Marco and T. Stanev, *Phys.Rev.* **D72** 081301, (2005): astro-ph/0506318.
- [11] M. Bertaina, for the EAS-TOP and MACRO Collaborations, *28th ICRC, Tsukuba 2003, Cosmic Rays*, 115 (2003).
- [12] T. Antoni *et al*, KASCADE Collaboration *Astropart. Phys.* **16**, 373, (2000).
- [13] O.A. Gress *et al*, TUNKA Collaboration *Proceedings of the 25th ICRC*, 129, (1997).
- [14] J. R. Horandel *et al*, KASCADE Collaboration, *Proceedings of the 26th ICRC*, 337, (1999).
- [15] M. Aglietta *et al*, EAS-TOP Collaboration *Astropart. Phys.* **10**, 1, (1999).
- [16] S.I. Nikolsky, *Nucl. Phys. Proc. Suppl.* **B 75A**, 217, (1999).
- [17] A. A. Petrukhin, *Proceedings of the XI Rencontres de Blois, "Frontiers of Matter"* Blois, France, (1999).
- [18] D. Kazanas and A. Nicolaidis, astro-ph/0103147.
- [19] D. Kazanas and A. Nicolaidis, *Gen.Rel.Grav.* **35**, 1117, (2003): hep-ph/0109247.

- [20] For a review and references, see J. Horandel, astro-ph/0508014.
- [21] B. Peters, Nuovo Cim. Suppl. **14**, 436, (1959).
- [22] K. H Kampert *et al* (KASCADE Collaboration) *Proceedings of the ICRC26*, OG.1.2.11; K-H Kampert *et al* (KASCADE Collaboration), Acta Phys.Polon. B **35** 1799, (2004)[astro-ph/0405608].
- [23] M. Aglietta *et al*(EAS-TOP Collaboration and MACRO Collaboration), Astropart. Phys. **20**, 641, (2004).
- [24] J. Candia and E. Roulet, JCAP **0309**, 005, 2003 [astro-ph 0306632].
- [25] I.S. Alekseev and G. T. Zatsepin *Proceedings of the ICRC1*, 326, (1960).
- [26] R. P. Kokoulin and A. A. Petrukhin, Sov. J. Part. Nucl **21**(3), 332 (1990).
- [27] R. P. Kokoulin and A. A. Petrukhin, Nucl. Instrum. Methods Phys. Res. A **263**, 468 (1988).
- [28] India-based Neutrino Observatory: Interim project report. Vol. 1. By INO Collaboration (V. Arumugam et al.). INO-2005-01, 2005. 200pp. See also <http://www.imsc.res.in/~ino>.
- [29] D. Muller *et al*, TRACER Collaboration, 29th ICRC Pune(2005) **3**, 89.
- [30] G. Navarra, *et al* Nucl. Instrum. Methods Phys. Res. A **518**, 207 (2004).
- [31] H. Falcke *et al* Nature, **435**, 313, (2005)
- [32] V. Berezhinsky, Nuclear Physics B (Proc. Suppl.) **151** (2006) 260-269.
- [33] G. Sigl, Lectures given at summer schools in Kopenhagen and Parma (2001), hep-ph/0109202.
- [34] R. Gandhi, Nucl. Phys. Proc. Suppl. **91**, 453, (2000): [hep-ph/0011176].
- [35] R. Gandhi, C.Quigg, M.H. Reno, I.Sarcevic, Astropart. Phys. **5**, 81, (1996)[hep-ph/9512364].
- [36] R. Gandhi, C.Quigg, M.H. Reno, I.Sarcevic, Phys.Rev. **D58**, 093009, (1998)[hep-ph/9807264].
- [37] T. Gaisser, F. Halzen and T. Stanev, Phys. Rept. **258**, 173, (1995).
- [38] F. Halzen, astro-ph/0604441.
- [39] A. Silvestri for the AMANDA Collaboration, Int. Jour. of Mod. Phys **A20**, 3096 (2005).
- [40] T. DeYoung for the ICECUBE Collaboration, Int. Jour. of Mod. Phys **A20**, 3160 (2005).
- [41] M. Circella for the NEMO Collaboration, ICRC, Pune, 2005.
- [42] E. V. Bugaev *et al* Phys. Rev. D **58**, 054001, (1998).

- [43] T. S. Sinegovskaya and S.I. Sinegeovsky, Phys. ReV. D **63**, 096004, (2001).
- [44] J. F. Beacom and J. Candia, JCAP **0411**, 009, (2004) [hep-ph 0409046].
- [45] L. V. Volkova, Sov. Jour. Nucl. Phys. **31** 784, (1980).
- [46] T.K. Gaisser *et al* Phys. Rev. **D38**, 85 (1988); G. Barret *al* Phys. Rev. **D39**, 3532 (1989).
- [47] P. Lipari, Astropart. Phys. **1** 195 (1993).
- [48] M. Thunman, G.Ingelman, P. Gondolo, Astropart.Phys. **5** 309 (1995).
- [49] M. Aglietta *et. al.*, LVD Collaboration, Phys. Rev. **D60** 112001 (1999).
- [50] M. Nagano *et. al.*, Journ. of Physics G: Nucl. Phys. **12** 69, (1986).
- [51] <http://amanda.berkeley.edu/>
- [52] E. Zas, F. Halzen and R. Vazquez, Astropart. Phys. **1** 297 (1993).
- [53] O Ryazhskaya, L. Volkova and O. Saavedra, Nucl. Phys. Proc. Suppl. **B 110**, 531, (2002).
- [54] L. Pasquali, M. H. Reno and I. Sarcevic, Phys. Rev. **D59**, 034020, (1999).
- [55] E. Bugaev, V. Naumov, S. Sinegovsky and E. Zaslavskaya, Nuovo Cim. **C12**, 41, (1989).
- [56] G. Gelmini, P. Gondolo and G. Varieschi, Phys. Rev. **D61**, 036005, (2000); *ibid.* Phys. Rev. **D61**, 056011, (2000).
- [57] A. Martin, M. Ryskin and A. Stasto, Acta Phys.Polon. **B34**, 3273, (2003)[hep-ph/0302140].
- [58] Gelmini *et al* Phys. Rev. D **67**, 017301, (2003) [hep-ph 0209111].
- [59] S. R. Kel'ner and Yu. D. Kotov, Sov. J. Nucl. Phys. **7** 237, (1968).
- [60] A. P. Chikatur *et al*, NuTeV/CCFR Collaboration ,Z.Phys.**C74**,279-290,1997
- [61] A. A. Petrukhin and V.V. Shestakov, Can J. Phys. **46**, s337(1968).
- [62] L. B. Bezrukov and E. V. Bugaev, Sov. J. Nucl. Phys. **33**, 635 (1981); E.V. Bugaev and Yu. V. Shlepin, Phys.Rev. **D67**, 034027, (2003) [hep-ph/0203096].